Transactions, **SMiRT-26**
Berlin/Potsdam, Germany, July 10-15, 2022
Division IX

MULTI-SENSOR CONCEPTION FOR SAFE SEALING STRUCTURES IN UNDERGROUND REPOSITORIES

Franziska Baensch[1], Detlef Hofmann[1], Sergej Johann[1], Carlo Tiebe[1], Frank Basedau[1], Patrick Sturm[1], Vera Lay[1], Ernst Niederleithinger[1]

[1] Bundesanstalt für Materialforschung und -prüfung (BAM), 12205 Berlin, Germany (vera.lay@bam.de)

ABSTRACT

The project "SealWasteSafe" of the Bundesanstalt für Materialforschung und -prüfung (BAM, Berlin) deals with sealing structures applied for underground disposal of nuclear waste from two perspectives: (1) material improvement for application in sealing constructions and (2) feasibility study regarding multi-sensor approaches to ensure quality assurance and long-term monitoring.

One specimen of 150 l made of alkali-activated material, which was found innovative and suitable for sealing constructions based on preliminary laboratory studies, and, for comparison purpose, another one made of salt concrete, are manufactured with an integrated multi-sensory setup for quality assurance and long-term-monitoring. The specimens were left in their cast form and additionally thermally insulated to simulate the situation in the repository. The multi-sensory concept comprises RFID technology embedded in the specimens suppling material temperature and moisture measurements, integrated fibre optic sensing allowing strain measurement and acoustic emission testing for monitoring possible crack formation. Overall, the suitability and the functionality of the sensors embedded into and attached to strongly alkaline (pH > 13 for the AAM) and salt corrosive (NaCl) environment was proven for the first 672 h.

First temperature measurement based on RFID succeeded after 626 h for the alkali-activated material and after 192 h for the conventional salt concrete. Strain measurement based on distributed fibre optic sensing turned out the alkali-activated material with > 1 mm m^{-1} undergoing approximately twice the compression strain as the salt concrete with strains < 0.5 mm m^{-1}. In contrast, the acoustic emission first and single hits representing crack formation in numbers, was found for alkali-activated material half of that detected at the salt concrete.

INTRODUCTION

Improving the construction materials of sealing structures and evolving approaches for their monitoring and inspection are the focus of the project " SealWasteSafe -Sealing Constructions for Underground Waste Disposal Sites: Safe Materials, Quality Assurance and Monitoring", BAM (2022). Sealing structures form engineered barriers that are crucial for nuclear waste repositories and need to fulfil high demands concerning integrity. Particularly in salt as a host rock, constructions made of salt concrete are suggested by BGE, the federal company for radioactive waste disposal (BfS, 2015). In addition to the material optimization and development of multi-sensory monitoring techniques, ultrasonic methods for inspection tasks at the engineered barriers are developed in this project. The large-aperture ultrasonic system (LAUS) is proven by Effner et al., (2021) to be capable to detect obstacles, possible cracks and delamination with depth penetration as high as 9 m at a test site in Morsleben by BGE. Complimentary, an advanced ultrasonic borehole probe is developed to allow for more detailed analysis from boreholes at the test site (Mielentz et al., 2021).

Among others, Li et al. (2020) showed that innovative alkali activated material (AAM) are characterized by particularly low thermally induced deformations during setting and hardening resulting, among others, less likely to crack. Less crack formation is a particular advantage for use in a repository since the sealing structure must prevent potential water and gas exchange between the radioactive waste and environment. After successful laboratory scale studies by Sturm et al. (2021) to obtain the most suitable AAM, larger scale test specimens of 100-3000 l were manufactured. The current contribution presents one 150 l specimen made of AAM, and, for reference reasons, another one made of a benchmark material, the so called “M2” salt concrete which was developed for the Morsleben disposal site in Germany (DBE, 2004). The specimen shape of a cylinder was chosen to be roughly comparable to the geometry of sealing structures, i. e. the back fill is taking place in caverns within the rock salt formations.

To monitor the materials’ setting and hardening processes in terms of quality assurance, and moreover, implementing and testing sensor setups for long-term monitoring, various non-destructive testing (NDT) methods are applied to both specimens: Besides wired reference sensors, also sensor systems based on wireless radio frequency identification technology (RFID), proven by Johann et al. (2021), are integrated into the material. Based on the expertise of Krebber and Habel (2011), distributed fibre optic sensors (FOS) were embedded to measure the strains at several positions at the cross area as well as along the specimens’ height. Acoustic emission (AE) testing is well known for crack detection in concrete. Moreover, Pirskawetz and Weise (2006) and Van den Abeele et al. (2009) investigated early age hydration processes of concrete. However, when applying AE regarding a reliable, secure evidence of the test object’s integrity, it must be installed from the very beginning of the component’s operation to allow the observation of possible crack formation and growth during setting, hardening, and aging of the materials.

For the long-term monitoring, the sensors were embedded into the materials, which is the most challenging part, because, in case of AAM and M2, the sensors must stay permanently stable in a strongly alkaline ($pH > 13$ for the AAM) and salt corrosive ($NaCl$) environment.

The current contribution focuses on the multi-sensory concept for monitoring setting and hardening processes of 150 l specimens made of AAM and M2.

EXPERIMENTAL DESIGN AND MULTI-SENSORY SETUP

The cylindrical specimens were manufactured by using PVC pipes (Ø 400 mm, 1200 mm length) as casting moulds (Fig. 1) with a time interval of 28 days (Tab. 1). Wired temperature and humidity sensors were also positioned near the RFID sensors for reference purposes. Embedded sensors such as the two RFID systems and the fibre optic sensors (FOS) were previously aligned and fixed in the PVC pipe using stretched nylon strings (Fig. 1c), whereby spacers kept the individual strands of the sensor fibre separated from each other.

Table 1. Overview of the measurements on AAM and M2

Material	AAM	M2
Water addition	April 21, 2021, 9:50 a.m	May 19, 2021, 10:02 a.m.
Peak in material temperature	29.0°C after 26 h	36.5°C after 108 h
End of measurement after 28 d	May 19, 2021 after 672 h	June 16, 2021 after 672 h

Filling the PVC form was handled manually within less than two hours. The specimens stood encapsulated by the PVC mould until finishing the measurements. Before starting the measurement, the specimens were thermally insulated with Styrofoam facade insulation panels (EPS 035 WDV 60 mm) to simulate the situation in the repository, i. e. with salt rock hardly conducting heat.

One specimen was made of AAM, and, for reference reasons, another one was made of a the so called “M2” salt concrete which was developed for the Morsleben disposal site in Germany (DBE, 2004).

The setting and hardening of both specimens were captured by a multi-sensory monitoring concept by integrating different sensors (Fig. 1).

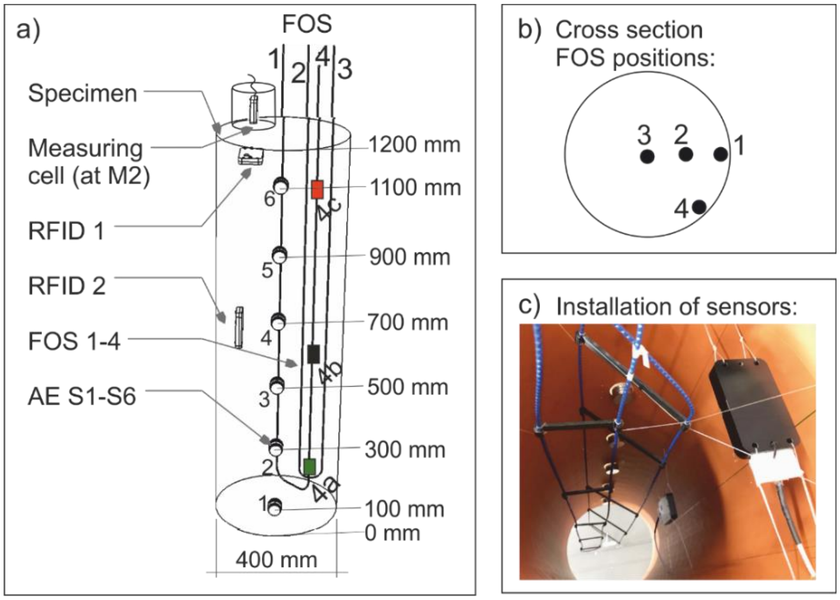

Figure 1. a) Coordinates of the sensors integrated in the specimen, b) Arrangement of the FOS at the cross-section c) Photography of the sensor installation before casting the specimen.

Cabled sensors for temperature and moisture references

Reference measurement of material temperature and material moisture were realized by integrating sensors in the immediate vicinity of each RFID transponder. HIH5030 sensors for humidity measurement with housings that are of comparable design to the housing of the RFID transponder were embedded for material moisture measurement and thermocouples type K with Teflon (PFA) coat were embedded for temperature measurement. The materials' temperature and moisture data were captured automatically once per hour. In case of the M2 specimen, the reference sensor was not integrated but positioned close to the specimen's surface on top in a separate measuring cell (Fig. 2a), which was sealed airtight from ambient climate as it was concreted in on one side of the sample surface.

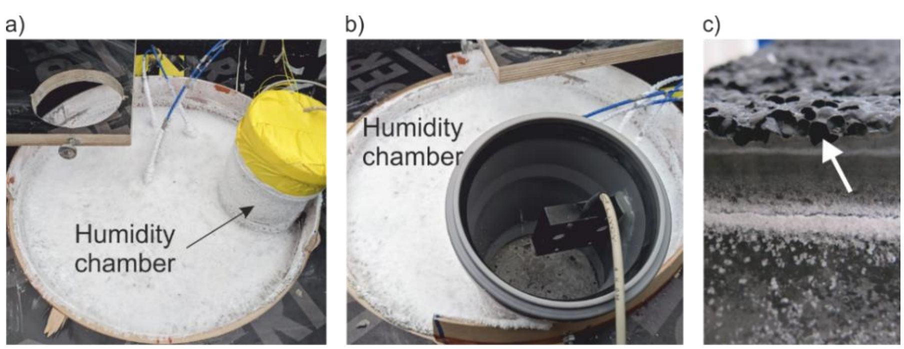

Figure 2. a) Surface of the M2 specimen with salt crust and partly embedded and sealed measuring cell with reference humidity sensor b) Opened measuring cell with reference humidity sensor wherein no salt crust was built c) Top layer of the AAM with an increased amount of air voids that did not escape the surface.

Integrated RFID Transponder

The advantage of applying RFID technology when embedding sensors in concrete materials is the absence of cables avoiding damage or weak points for water exposure. Moreover, its passive mode of operation makes RFID technology attractive to long-term monitoring applications. To ensure functionality of the sensor against harsh environment and values of pH > 13, its housing must meet special requirements, especially when already integrated preliminary to casting the concrete.

An SL13A transponder with temperature sensor is supplemented by a HIH5030 sensor for humidity measurement (Fig. 3). The housing of this setup is made of PVC and has 112 x 66 x 18 mm³ dimensions. To enable moisture transport from the enclosing material into the casings inside with the integrated sensor, an interface (Ø 10 mm) is realized by implementing a filter (100 µm) of polytetrafluoroethylene (PTFE). Further details are discussed by Johann et al. (2021). The power measurement was performed using the Tagformance® Pro measurement system from Voyantic. The here employed high frequency RFID technology allows embedding at a depth of less than 100 mm. In the here presented study, the sensors were embedded 60 mm from specimen surface.

RFID measurements were carried out manually daily until the measure succeed once a week, and then continued sporadically and less frequently. These RFID sensors will continue to be studied for long-term monitoring.

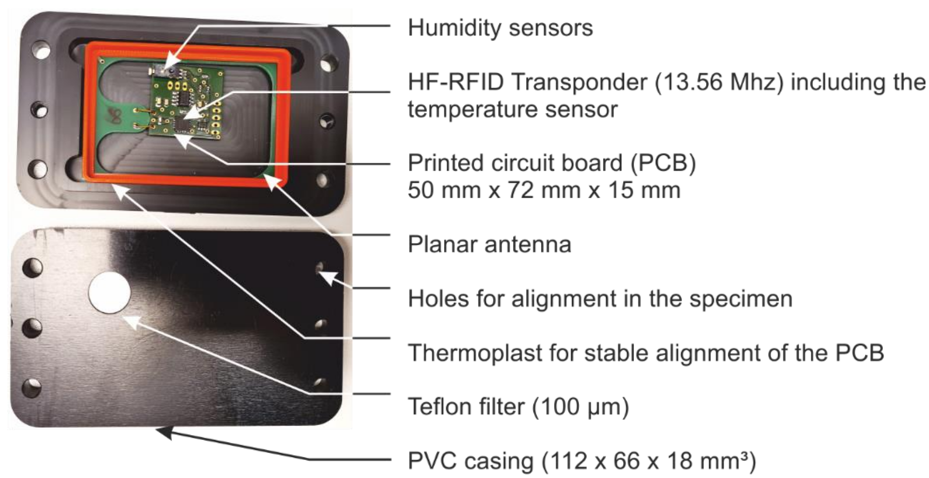

Figure 3. RFID transponder including temperature and humidity sensors

Integrated Distributed FOS Technology

For embedding FOS in harsh environments, the sensor type BRUsens DSS 3.2 with its coating of Polyamid was found of adequate stability. The FOS was arranged at four different positions over the cross section and distributed along the specimen's length (Fig. 1). This allows information on the specimen's deformation in the centre and along its axis of rotation as well as near the edge. To determine the strains at different heights of the specimens, short measuring sections of 40 mm in length were evaluated along one of the four fiber section over cross section (Fig. 1a, 4a-4c). Here, the FOS 4 (Fig. 1b) is evaluated for both specimens. The distributed FOS based on Rayleigh backscattering was performed with the LUNA OBR System. A spatial resolution of 5 mm and a high resolution of 1 µm m^{-1} in strain were yielded. Strain monitoring was realized by one measurement each hour.

Appliqued AE Monitoring

To enable detection of crack formation, AE monitoring was implemented. The AE acquisition was performed with an AMSY6 in threshold-based mode with a recording rate of 10 MHz, 16384 samples per data set and a frequency filtering from 20 kHz to 500 kHz. Six piezo-electric sensors type VS45H were placed along the specimens' heigh by 200 mm distances to realize a rather zonal location of AE activity (Fig. 1a, S1-6) during setting and hardening of the specimen.

In contrast to RFID and FOS, the AE measurement is more suitable to be applied externally. Stainless steel cylinders (Ø 40 mm, 18 mm anchoring depth) were manufactured as "AE adapters" and have been intruded into the test specimen like an anchor protruding halfway to allow coupling of the sensors. Before casting, these AE adapters were screwed to the PVC pipe using mounting plates. After the specimen has hardened, these one-way embedded AE adapters are positively connected with the specimen and the holder plates have been removed. Thus, AE adapters have no contact with the PVC pipe anymore. AE monitoring was online enabling AE hit detection by crossing the predefined threshold of 45 dB. To ensure that each original event is only counted once in AE analysis, the arrival time differences are determined in the case of multiple detections (location procedure for a rod, VisualAE ™ from Vallen Systeme GmbH). Thus, the databases consist of AE that were detected only by one single sensor as well as the first hits of multiple detected AE. In the following section, the results of the sensors S1, S3 and S6 are presented exemplarily.

RESULTS AND DISCUSSION

Material temperature and moisture measurement

For AAM, the peak temperature was yielded after 26 h. After 96 h, the temperature is still dropping, and then, after 192 h (8 days) reached the equilibrium within the insulating housing approximately (Fig. 4a). The relative humidity inside the thermal insulation falls to approximately 25 % (Fig. 4b) during the first 24 h after casting. Thereafter, the measured material moisture increased up to 75% without decreasing for the following 27 days. This is in accordance with the results found by Hu et al. (2020), who also observed a comparable increase of the internal relative humidity due to condensation reaction of comparable alkali-activated material.

In case of M2, after 96 h, the temperature curve was still rising. Its peak was yielded after 108 h and the temperature was adjusted to the temperature within the housing approximately after 323 h (13 days) (Fig. 5a). Inside the thermal insulation, after casting the M2 specimen, the humidity decrease took about 100 h (Fig. 5b). After 672 h 30 % humidity was measured inside the insulation. The material moisture was measured in an airtight measuring cell at the specimen's top surface (Fig. 2a), but not embedded in the material in 60 mm depth. Within the first 24 h the measured material moisture increased up to 75 % and remained on a constant level slightly altering for the following 27 days. Note that the reference sensor casing (Fig. 2b) is comparable to the one designed for the RFID shown in Fig. 3 and follow the discussion within the next subchapter concerning the results from RFID measurements.

Results From Integrated RFID Technology

For performing the RFID measurement, power transmission is required, whereby water, as it occurs when casting the specimens, is a barrier and makes measurement difficult to impossible during the setting of the material.

For the AAM, a first successful RFID measurement was carried out after 626 h (26 days), yielding comparable temperature values as by calibrated and cabled reference measurement (Fig. 4a). However, unreasonably more than 100% moisture were measured by means of the RFID (Fig. 4b). The first RFID measurement at the M2 succeeded only after 198 h (8 days), whereby the temperature was found in good correlation to the reference material temperature (Fig. 5a). Comparable to the humidity measurement at the AAM, the RFID and the reference output are non-realistic (Fig. 5b).

Employing the RFID for temperature measurement works well, whereas the humidity measurement faces further challenges. In general, the functionality of RFID sensors to monitor moisture in concrete has been proven by Strangfeld et al. (2017) and Johann et al. (2021). However, the weak spot in the design is the filter, which is needed for the moisture and gas exchange between sensor casing and material but allows the casing to be flooded during casting the specimen. It is assumed, that moisture is enclosed in the PVC casing of the RFID transponder, only leaking very slowly and by this, reaching the equilibrium with the surrounding material. Thus, realistic material moisture measurements are expected after several months of material aging. If not so, another assumption is that the filter material of the housing is clogged by a layer of salt, potentially causing the moisture sensor to malfunction. Finally, the specimens might be opened at some time in future to evaluate the sensors' functionality and durability within the strongly alkaline concrete (pH > 13).

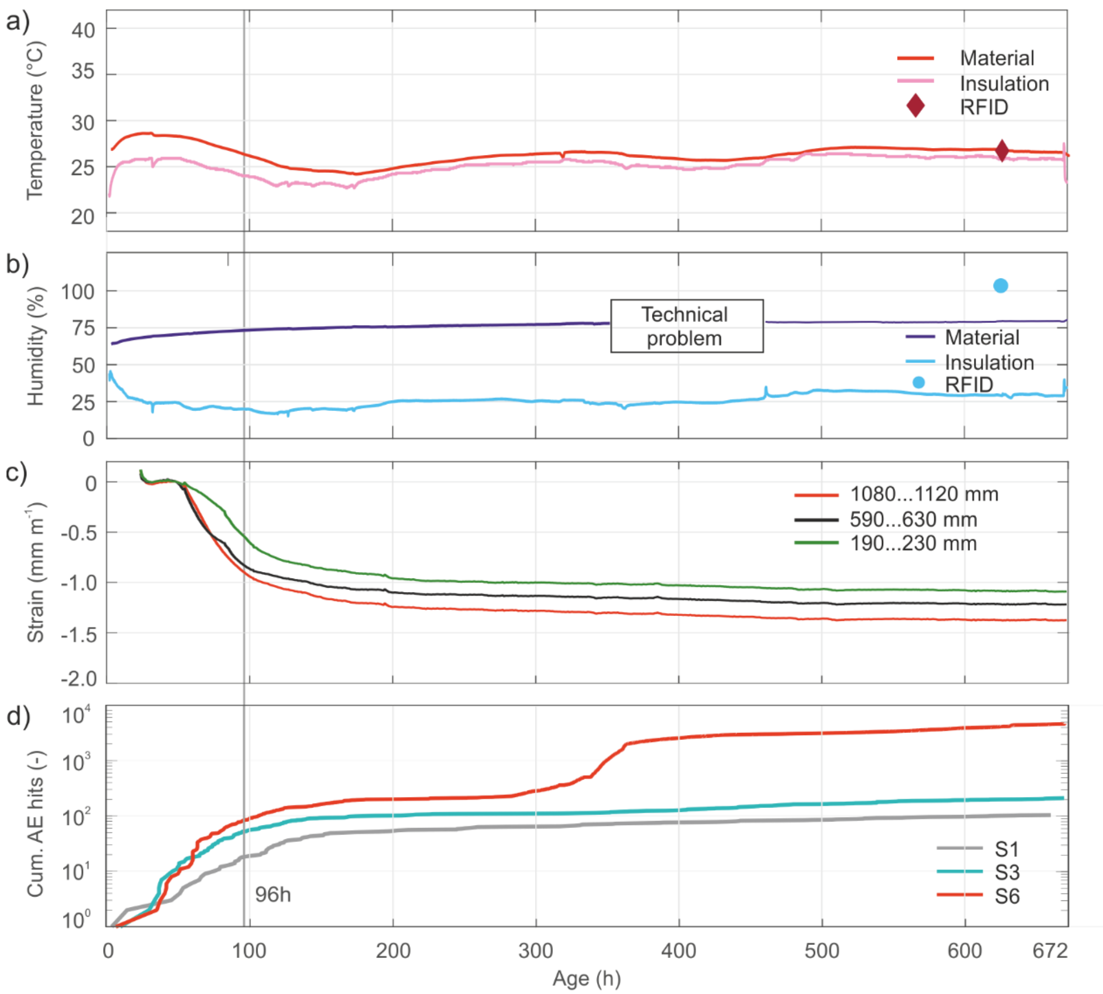

Figure 4. 28 days monitoring of the AAM: a) Material temperature from cabled reference and RFID vs. temperature inside the insulation. b) Material moisture from cabled reference and RFID vs. humidity inside the insulation. c) Strain from FOS 4 of three different heights. d) AE activity detected by sensors. S1, S3 and S6.

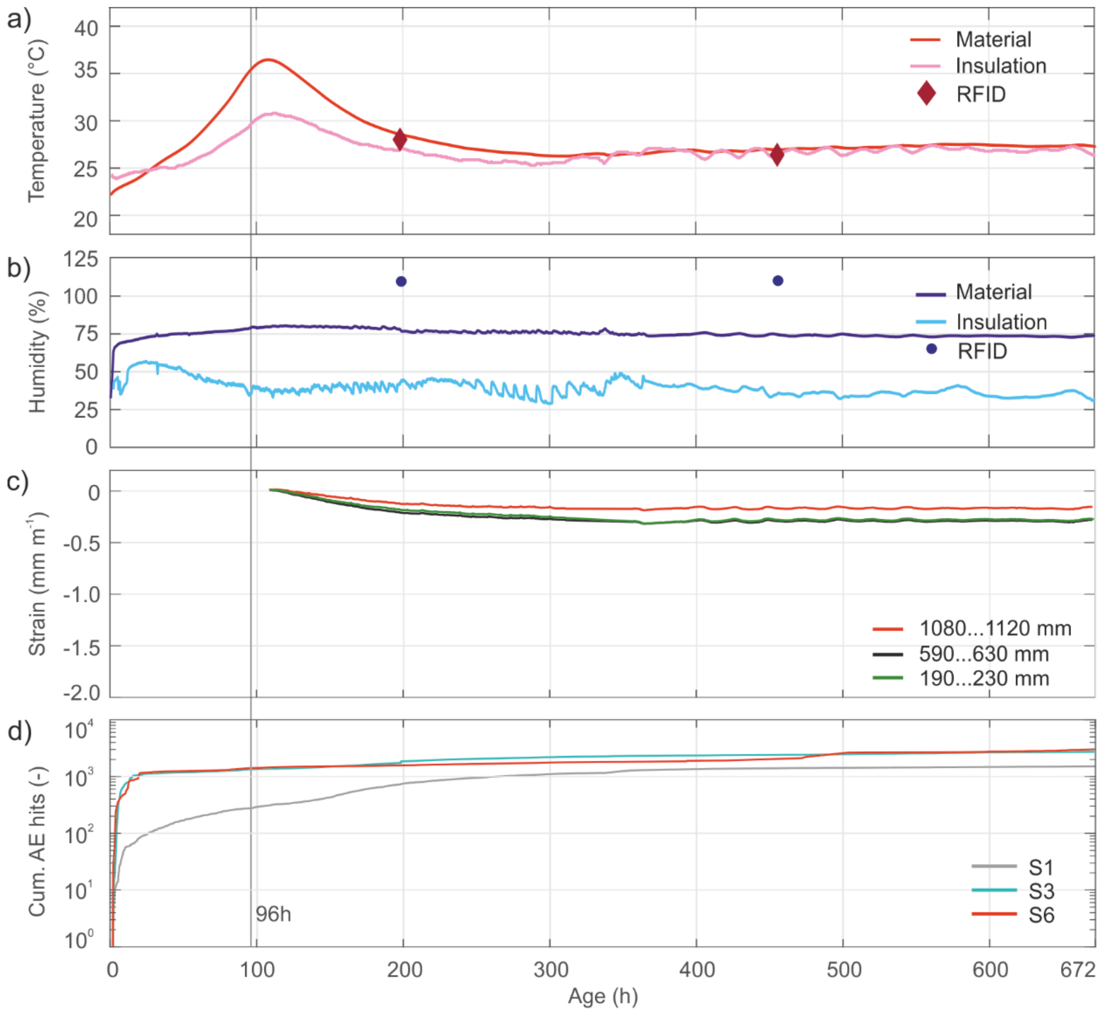

Figure 5. 28 days monitoring of the salt concrete: a) Material temperature from cabled reference and RFID vs. temperature inside the insulation. b) Material moisture from cabled reference and RFID vs. humidity inside the insulation. c) Strain from FOS 4 of three different heights. d) AE activity detected by sensors. S1, S3 and S6.

Results From Integrated FOS Technology

For the overall view of both specimens, the strain profiles measured based on embedded FOS followed the material's temperature profiles (Fig. 4a, c, Fig. 5a, c). The zero value in FOS strain was set synchronously to the temperature maximum, which was reached for AAM after 24 h and for M2 after 108 h. Strain values based on FOS are only evaluable from this starting points.

During the first 672 h, with strain measurements starting as soon as the maximum temperature was reached, the AAM specimen underwent more pronounced maximum compression strains of 1.3 mm m^{-1} (Fig. 4c, 1080…1120 mm), whereas at the M2 specimen less than 0.5 mm m^{-1} were measured (Fig. 5c). This more pronounced strain is common for AAM because during the hardening water is released within condensation reaction and thus the initial volume of the test specimen shrinks. This specific shrinkage mechanism does not apply to M2 to this extent because more of the reaction water is included to the reaction products (hydration). However, the significant deformation of 0.9 mm m^{-1} were measured after 96h. Afterwards, the AAM underwent progressive compression by further 0.4 mm m^{-1} strain, which is comparable to the compression strain of approximately 0.3 mm m^{-1} for the M2 between 108 h to 672 h.

For the AAM, the highest compression was detected at the top position of the specimen and the lowest at the bottom, whereby the strain profile at the bottom has been thwarted at 50 h to 80 h of material aging (flatter decrease, see Fig. 4c). In case of the M2, at middle and bottom positions comparable compression strains were yielded, whereas at the top of the specimen a significantly lower compression was measured (Fig. 5c). After 393 h, a periodic variation of the strain values was observed for M2 possibly following the variation in temperature inside the insulation (Fig. 5a).

Cumulative AE Activity

The cumulative AE activity counts the number of hits detected during the monitoring for 672 h. Generally, a rather distinct trend to build cracks generated a relatively high number of AE. Compared to the M2 specimen that generated 16740 AE events, 6105 AE events were detected for the AAM, which is less than half as much. During the setting within the first hours and days of the specimens, AE may have been generated also by phase transition to a not inconsiderable extent. Whereas 96 h after casting, during hardening, AE is assumed to be mainly generated by crack formation and growth for both materials. Between 96 h and 672 h, 5487 AE (single and first) hits, cumulated over all sensors, were detected at AAM, 82% of it at sensor 6 (Fig. 6a). In contrast, for M2 significantly more AE activity was detected, since all six sensors together detected 9407 AE hits during 96-672h after casting (Fig. 6b).

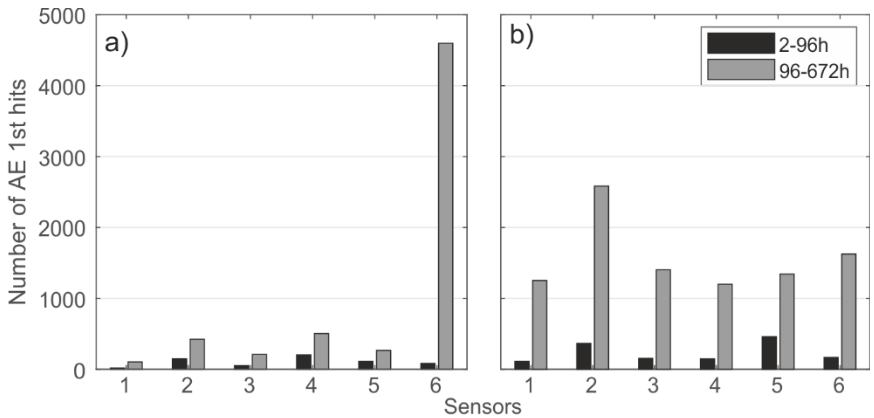

Figure 6. Number of AE first hits at the sensors S1-S6 detected at the a) AAM specimen and the b) salt concrete cumulated between 2-96 h and 96-672 h after casting.

For the AAM, the threshold of 100 AE hits detected at each sensor (S2-S6), was crossed between 60 h and 130 h (Fig. 4d), which is in good correlation with decreasing material temperature and strain values, possibly indicating the shift from setting to hardening processes, which is a continuous transition for this material. The increase in AE activity at S6 between 290 h and 370 h might have been caused by increased crack formation at the specimen's bubble-like surface (Fig. 2c), which is a result of entrapped air from mixing that did not fully escape through the hardening surface of the specimen.

M2 crossed the 100 hits per sensor during the first 12 h after casting, and S3-6 yielded approximately 1000 AE hits within the first 24 h (Fig. 4d). At the bottom region of the specimen, a significantly lower AE activity level and slower increase was detected at S1-2. For the M2 another increase in AE activity at S6 between 472 h and 500 h was detected, possibly generated by crack formation due to drying, comparable as for the AAM and favoured by accumulated fines because of sedimentation of bigger particles of the very fluid fresh material.

CONCLUSION AND OUTLOOK

To enable safer underground sealing structures for nuclear waste disposal, the setting and hardening of two 150 l cylindrical specimens made of alkali-activated material (AAM) and M2 salt concrete were monitored for the first 672 h after casting based on a multi-sensory approach. By this, suitability and functionality of the sensors embedded into and attached to strongly alkaline (pH > 13 for the AAM) and salt corrosive (NaCl) environment was proven for the first 672 h.

Based on cabled reference measurement, the less exotherm setting time of AAM yielding its peak temperature during the first day (Fig. 4a) was proven in comparison to the M2 with its maximum temperature four days after casting (Fig. 5a). For both materials, the material moisture of approximately 75 % was measured by the cabled reference sensors, which is in accordance, at least for AAM, with the recent literature. Moreover, the drop of the relative humidity yielding the equilibrium inside the insulations were found in temporal correspondence with the materials' maximum temperatures.

Based on RFID technology, the first measurement succeeded after 26 days at the AAM and after 8 days at the M2 specimen. However, while temperature values were in correlation to the reference measurements, unrealistic humidity values were detected. Thus, the humidity measurement faces further challenges. Future investigations will focus on further improvements of the sensor design regarding the filter for the RFID casing to enable secure long-term material humidity measurements in harsh environments.

The curves of compression strain based on the FOS measurement followed the material temperature curves. During the first 672 h, the AAM specimen underwent more pronounced compression strains of more the 1.0 mm m^{-1} (Fig. 4c), whereas at the M2 specimen less than 0.5 mm m^{-1} were measured (Fig. 5c). The determination of deformation along the specimens' heights identified the lowest compression strain at the bottom position for the AAM, but at the top position for the M2.

The AE activity (cumulative number of first hit AE) detected for AAM was approximately half of that detected at the M2; under similar conditions. For both materials, the lowest AE activity was detected at the bottom (Fig. 4d, S1 and Fig. 5d, S1).

The linkage of the results from FOS and AE during the hardening, which occurred after 96 hours with both materials, most likely reveals a different cracking behaviour of the two materials, since both underwent strains in the same range, but the AAM generated less AE (cracks) than the salt concrete during 96 – 672 h (Fig. 6). Physically, more strain with less cracking correlates with higher ductility and lower Young's Modulus. Since, for the AAM, the main part of the compression strain occurred during setting, cracking possibly is prevented by the early ductility. However, further studies are required to substantiate this hypothesis.

Future investigation will focus on evaluating the invasive impact on the specimens by integrated RFID and FOS technologies by employing further non-destructive methods like ultrasound measurements, computer tomography or thermographic measurements. Moreover, further studies regarding long-term monitoring are still ongoing.

ACKNOWLEDGEMENT

The authors thank Kerstin Borchardt-Giers, Marco Lange and Sean Smith for manufacturing the molds and equipment for insulating the specimens, Frank Haamkens and Stefan Schacht for manufacturing the AAM and the M2 specimens, Marcus Thomas for calibrating the reference temperature sensors, Samuel Pötschke und Mathias Breithaupt for helping integrating the FOS sensors, Heiko Stolpe and Christoph Strangfeld for producing the reference humidity sensors, Harald Kohlhoff for designing and manufacturing the RFID casings and the AE adapters.

REFERENCES

Bundesamt für Strahlenschutz, „Endlager Morsleben: Hintergründe, Maßnahmen und Perspektiven der Stilllegung“, 2015, LINK: https://archiv.bge.de/archiv/www.endlager-morsleben.de/SharedDocs/Downloads/Morsleben/DE/broschueren/morsleben-stilllegung-neuf4b0.pdf?__blob=publicationFile&v=9

Bundesanstalt für Materialforschung und –prüfung, Berlin, 2019-2022, *https://www.bam.de/Content/DE/Projekte/laufend/SealWasteSafe/seal-waste-safe.html*

Deutsche Gesellschaft zum Bau und Betrieb von Endlagern für Abfallstoffe mbH (DBE), “Verfüllmaterial für Strecken mit hohen Anforderungen Materialeigenschaften und Materialkennwerte Salzbeton M2“, *Bundesamt für Strahlenschutz, Salzgitter, 2004*

Effner, U., Mielentz, F., Niederleithinger, E., Friedrich, C., Mauke, R., & Mayer, K.: Testing repository engineered barrier systems for cracks - a challenge. *Materialwissenschaft und Werkstofftechnik, 52(1), 19-31, doi: 10.1002/mawe.202000118*, 2021.

Hu, z., Wyrzykowski, M., Lura, P., “Estimation of reaction kinetics of geopolymers at early ages”, *Cement and Concrete Research 129 (2020) 105971, https://doi.org/10.1016/j.cemconres.2020.105971*

Johann, S., Baensch, F., Sturm, P., Tiebe, C., Pötschke, S., Lay, V., “HF RFID-based Measurement Comparison for Method Optimization in M2 Concrete and Alkali-Activated Mortars” *35th Danubia - Adria Symposium on Advances in Experimental Mechanics*, *21.-24.09.2021, Linz, Österreich*. ISBN: 978-3-9504997-0-4

Krebber, K., Habel, W. “Fiber-Optic Sensor Applications in Civil and Geotechnical Engineering”, *Photonic Sensors (2011) Vol. 1, No. 3: 268–280*.

Li, Z. Zhang, S., Liang, X., Ye, G., “Cracking potential of alkali-activated slag and fly ash concrete subjected to restrained autogenous shrinkage“, *Volume 114, November 2020, https://doi.org/10.1016/j.cemconcomp.2020.10376.*

Mielentz, F., Stolpe, H., Effner, U., Behrens, M., Bernstein, T., Niederleithinger, E., „Entwicklung einer Bohrlochsonde für Ultraschalluntersuchungen an Abschlussbauwerken in Endlagern“ *Jahrestagung Deutsche Gesellschaft für Zerstörungsfreie Prüfung 2021, virtuell.*

Pirskawetz, S., Weise, F., “Detection of early-age cracking using acoustic emission”, *International RILEM Conference on Volume Changes of Hardening Concrete: Testing and Mitigation, RILEM Publications SARL, 2006, pp. 385 – 392, doi: 10.1617/2351580052.041*

Strangfeld, C., Johann, S., Müller, M., Bartholmai, M., “Embedded passive RFID-based sensors for moisture monitoring in concrete“, *2017 IEEE SENSORS, 2017, pp. 1-3, doi: 10.1109/ICSENS.2017.8234166.*

Sturm, P., Move, J., Gluth, G.J.G., Vogler, N., Taffe, A., Kühne, H.-C. “Properties of alkali-activated mortars with salt aggregate for sealing structures in evaporite rock” *Open Ceramics 5 (2021) 100041*.

Van Den Abeele, K., Desadeleer, W., De Schutter, G., Wevers, M. “Active and passive monitoring of the early hydration process in concrete using linear and nonlinear acoustics“, *Cement and Concrete Research 39 (2009) 426–432, doi:10.1016/j.cemconres.2009.01.016.*